ACS Catalysis

Research Article

pubs.acs.org/acscatalysis

Dimensionally Stable Ru/Ir/TiO_2-Anodes with Tailored Mesoporosity for Efficient Electrochemical Chlorine Evolution

Nadine Menzel, Erik Ortel, Katharina Mette, Ralph Kraehnert,* and Peter Strasser

The Electrochemical Energy, Catalysis, and Materials Science Laboratory, Department of Chemistry, Chemical Engineering Division, Technical University Berlin, Straße des 17. Juni 124, 10623 Berlin, Germany

ABSTRACT: Chlorine evolution is one of the most important electrochemical reactions applied in industry. We present a method for the synthesis of chlorine evolution catalysts with improved performance. The performance increase results from the introduction of controlled mesoporosity into the pore system of Ru- and Ir-containing TiO_2 catalysts by pore templating with micelles of amphiphilic block-copolymers. Micelle-templated TiO_2-based catalysts were synthesized with loadings up to 15 wt % of either Ru, Ir, or a combination of both active metals. The catalysts' walls are composed of nanocrystalline mixed oxides with rutile structure. The templated mesopores are about 10 nm in size and form an ordered cubic pore system with good pore connectivity. All studied catalysts are active in chlorine evolution. Adding templated mesoporosity doubles the catalyst performance at identical catalyst composition. The influences of film thickness, composition, and porosity of the developed catalytic coatings on the catalytic performance are discussed.

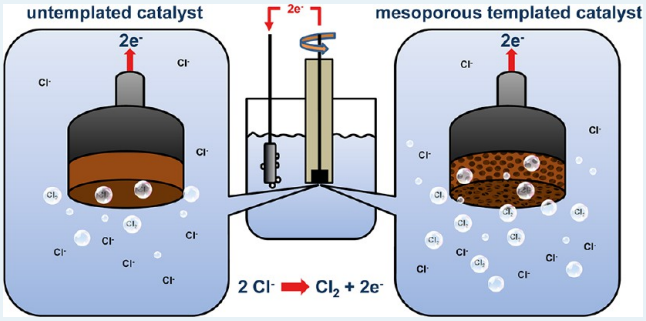

KEYWORDS: *mesoporous films, chlorine evolution, ruthenium oxide, iridium oxide, titanium oxide*

INTRODUCTION

The chlorine evolution reaction (ClER) is one of the most important practical applications of electrochemical reactions carried out on an industrial scale. In this reaction, sodium chloride is electrolyzed producing chlorine gas at the anode as well as sodium hydroxide and hydrogen at the cathode. About 10 million tons of chlorine are produced in Europe every year.[1] Chlorine is commonly used as intermediate for the production of polymers, disinfectants, and drugs.[1] Moreover, chlorine reduction is also used in hydrogen-chlorine regenerative fuel cells.[2,3]

Industrial chlorine evolution is performed on so-called "dimensionally stable anodes" (DSA), i.e., on electrodes for which corrosion and other degradation processes progress only slowly under electrochemical reaction conditions.[4] Dimensionally stable anodes therefore consist of materials for which electrode degradation is limited to the electro-active surface layer. Commonly employed electrode materials are, e.g., ruthenium/titanium mixed oxides or ruthenium/iridium/titanium mixed oxides.[5,6] Although oxygen evolution is thermodynamically favored ($E°$ = 1.26 V vs NHE) over chlorine evolution ($E°$ = 1.36 V vs NHE) under typical ClER conditions, it is slow due to kinetic limitations on this type of electrodes.[7]

Typical oxide electrodes for the chlorine evolution reaction are composed of mixed oxides of ruthenium−titanium or ruthenium−iridium−titanium. Especially Ru−Ti−O_x mixed oxides show a high catalytic performance toward chlorine evolution. Unfortunately, these electrodes degrade under harsh working conditions (high current densities and temperatures, low pH). To increase the lifetime and stability of such catalysts, iridium oxide is often added to the catalyst composition.[8,9] The most common method for the synthesis of Ru−Ti−O_x[10,11] or Ru−Ir−Ti-O_x[12] catalysts is the dissolution of ruthenium chloride, iridium chloride, titanium chloride, or di-isopropoxide bis-2,4-pentanedionate[12] in solvents (e.g., isopropanol,[12] propanol,[11] water[10]) followed by brushing of the solution onto an electrode substrate, drying, and finally thermal treatments to convert the deposit into ruthenium oxide. The coated electrodes usually possess a compact morphology[8] featuring mud-cracks within the coating. Depending on the synthesis procedure the oxide coatings can also contain textural porosity. The morphology of the electrode coating can be influenced by varying the coating technique like brushing, dipping, or spinning.[13]

The role of mud-cracks in chlorine evolution on oxide electrodes was studied by Evdokimov,[14,15] Gorodetskii,[16] and Panic.[17] They suggested that at high current densities the gas evolution takes place not only at the coatings outer surface but also inside of the pores that are provided by the textural porosity of the studied coatings. Furthermore the authors suggested that pores are necessary to enable a sufficiently fast chlorine removal at high current densities from the electrode due to the formation of gas channels inside the pores.

Received: January 11, 2013
Revised: April 23, 2013
Published: May 16, 2013

   dx.doi.org/10.1021/cs4000238 | ACS Catal. 2013, 3, 1324−1333

Unfortunately, reports on the synthesis of ClER catalysts with controlled and tunable mesopore size and studies on the corresponding effect of modified mesoporosity on ClER performance remain rather scarce.

Chen et al.[18−20] and Trieu et al.[21] studied the microstructural impact of the catalyst coating synthesizing supported nanoscale $Ru_xTi_{1-x}O_2$ (3 nm) on inert anatase TiO_2 (20 nm) by combining sol−gel with a solvothermal route.[18] The obtained coatings catalyzed the ClER at a 120 mV lower electrode potential than commercial $Ru_{0.3}Ti_{0.7}O_2$ catalyst coating. Moreover, also nanoporous compact $Ru_{0.3}Sn_{0.7}O_2$ was observed to be more active for ClER than a commercial $Ru_{0.3}Ti_{0.7}O_2$ catalyst.[19] A relation between the evolution of chlorine bubbles and the microstructure of the coating was reported, also for $Ru_{0.25}Ti_{0.7}V_{0.05}O_x$ coatings[20] synthesized via a sol−gel process and applied to the Ti substrate by drop- or dip-coating. An open surface morphology (e.g., cracks) was concluded to be important for gas bubble transport from the electrode surface. Mud-cracked TiO_2−RuO_2 and TiO_2−RuO_2−IrO_2 catalysts produced via electrodeposition[21] were reported to lower the chlorine overpotential by 90 mV at a current density of 400 mA/cm^2.

For other electrocatalytic reactions the synthesis of catalysts with defined mesopore structure has been reported recently.[22] Introducing, for example, templated mesopores into iridium dioxide improved its catalytic performance in oxygen evolution (OER) significantly and decreased the electrochemical overpotential.[22,23] The increased performance of porous catalysts can be attributed to three main effects: (i) an increase in electrochemically active surface area provided by the mesopore surface, (ii) improved diffusional access of electrolyte to the electrode surface, and (iii) faster transport of the evolving gas from the reactive pore surface due to enhanced pore connectivity.

Control over pore size and pore connectivity of oxide coatings can be achieved when the catalyst synthesis is supported by structure-directing agents. Micelles of amphiphilic block-copolymers are the most common agents employed in the synthesis of mesoporous metal oxides. In a typical synthesis, a solution containing a micelle-forming block-copolymer along with metal-oxide precursor(s) and a volatile solvent is deposited on a substrate followed by calcination. Under suitable coating conditions the volatile solvent evaporates during film deposition, whereas the remaining template molecules form micellar structures in a process called evaporation-induced self-assembly (EISA).[24,25] The micelles assemble along with the partially hydrolyzed and condensed oxide precursor into an ordered mesophase. A subsequently applied thermal treatment induces crystallization of the oxide framework as well as the removal of the pore template, yielding a mesoporous oxide coating with narrow pore-size distribution and nanocrystalline walls.[24,25]

The micelle-templated synthesis of mesoporous catalytic electrode coatings with compositions relevant to chlorine evolution has been reported so far for different metal oxides[26] including pure, IrO_2,[23] RuO_2,[27] and TiO_2.[28−31] Ortel et al. prepared mesoporous IrO_2 employing iridium acetate as precursor and PEO-PB-PEO triblock-copolymer as template.[23] Mesoporous RuO_2 thin films were synthesized by Sassoye et al. via dip-coating of solutions containing the precursor $RuCl_3{\cdot}xH_2O$ and the template PS-PEO.[27] Electrochemical cycling of the films in different electrolytes indicated an enhanced capacitance (0.1 M H_2SO_4) and ClER activity (0.1 M NaCl) arising from the crystalline mesoporous framework. Sugimoto et al. obtained ordered mesoporous ruthenium oxide powders by lyotropic liquid crystal templating starting from solutions containing BRIJ 56 and $RuCl_3$.[32] The ruthenium ions were reduced to metallic Ru by addition of Zn for 1 week followed by EtOH washing to remove the surfactant and acid leaching to remove Zn. The resulting powder was used to prepare and cast an ink and only thereafter electrochemically oxidized to obtain mesoporous RuO_2. Oh et al. produced RuO_2 powders with roughly 2 nm pore size from hexadecyltrimethylammonium chloride (surfactant) and Ru(III) nitrosyl nitrate (precursor) after precipitation, washing, and subsequent calcination at 200 °C for 48 h.[33] The high electrochemical capacitance measured for an ink prepared from the obtained RuO_2 powders was attributed to the obtained porosity increase. Titania films with micelle-templated large mesopores and also bimodal porosity[28,30] were reported by different researchers as reviewed recently by Pan et al.[31] However, the micelle-templated synthesis of mesoporous mixed oxides with compositions that promise the best ClER performance, i.e., Ru−Ir−TiO_x, has not been reported so far.

The present contribution demonstrates the first successful synthesis of mixed-oxide electrodes of composition ruthenium−iridium−titanium oxide with micelle-controlled mesopore structure and elucidates the influence of catalyst composition and mesopore structure on ClER performance. The developed synthesis employs EISA based on metal chlorides and acetate precursors along with commercial block-copolymers from the Pluronic family. Physicochemical material properties were analyzed via BET, SEM, EDX, XRD, and SAXS. The synthesized materials were tested as catalysts for ClER via cyclovoltammetric measurements from 1.2 to 2.0 V vs RHE (short time experiments) in the regime of bubble formation using a rotating disc electrode. Employing the developed strategy pore size, layer thickness and catalyst composition of the synthesized electrodes was varied to elucidate the influences of these parameters on the electrode performance in chlorine evolution.

EXPERIMENTAL SECTION

Chemicals. $TiCl_4$ (99.9%) and Pluronic F127 were purchased from Sigma-Aldrich. Ruthenium(III)acetate (42.23% Ru) and iridium(III)acetate (99.9%, 48.76% Ir) were obtained from Hereaus. All chemicals were used without further purification.

Synthesis of Mesoporous Oxide Coatings. Micelle-templated oxide coatings were synthesized with compositions Ru/TiO_2, Ir/TiO_2, and Ru−Ir/TiO_2 and with loadings varying between 0 and 15 wt % of Ru and Ir in titania. The coating solutions for the micelle-templated oxides were prepared by first dissolving titanium(IV)tetrachloride (1.0 g) in ethanol (5.0 mL). Then the respective amounts of ruthenium(III)acetate or iridium(III)acetate or both were added to the solution. The required amount of the Ir and Ru precursor was calculated to obtain a content of 5, 10, or 15 wt % of the metal (not oxide) in TiO_2. Moreover, 0.75 g of the template polymer F127 (PEO_{106}-PPO_{70}-PEO_{106}, 0.75 g) was dissolved in a mixture of ethanol (5.0 mL) and distilled water (0.83 mL) and then added to the precursor solution. As a reference, coatings without templated mesoporosity were prepared by dissolving titanium(IV)-tetrachloride (1.0 g) and the required amount of iridium(III)-acetate in ethanol (10.0 mL) and distilled water (0.83 mL).

dx.doi.org/10.1021/cs4000238 | ACS Catal. 2013, 3, 1324−1333

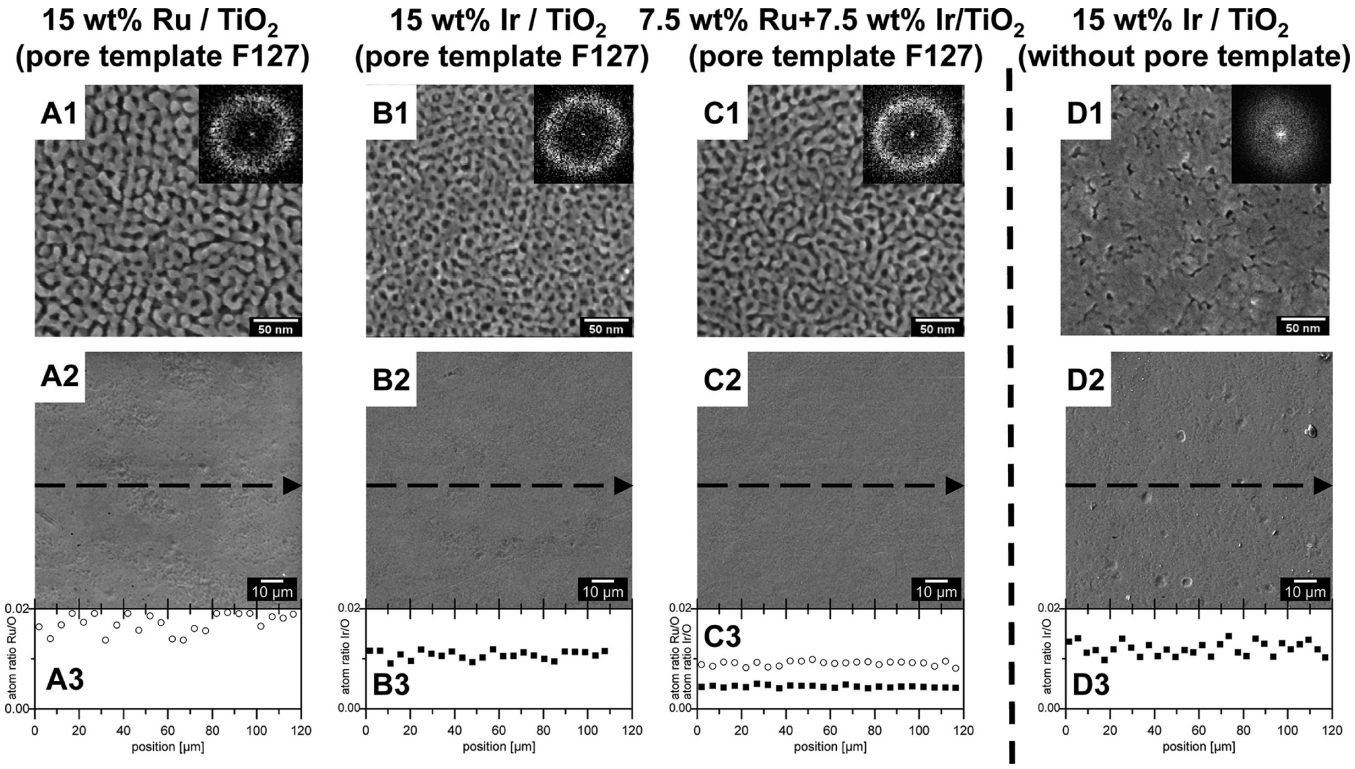

Figure 1. SEM analysis of F127 templated TiO_2-based catalyst films. Films contain (A) 15 wt % Ru, (B) 15 wt % Ir, and (C) 7.5 wt % Ru + 7.5 wt % Ir. (D) For comparison, an untemplated Ir/TiO_2-film containing 15 wt % Ir. Imaging performed at a magnification of 100,000× (row 1). Insets show the FFT of the respective image. Corresponding SEM images at a magnification of 1000 are shown in the row 2 together with an EDX line scan as graph (atom ratio of noble metal (Ir, Ru) and oxygen vs position) in row 3. All films were dip-coated onto titanium substrates at 60 mm/min and calcined at 475 °C.

Oxide coatings were synthesized on different substrates. For analysis, Si wafers as well as Ti foils (11.4 μm thickness, 99.6% Alfa Aesar; and 1.0 mm thickness, 3.7025 Gemmel) were employed, whereas titanium cylinders (5 mm in diameter and 4 mm in height) served as substrate for electrocatalytic RDE testing. The titanium cylinders were pretreated by grinding the front side of the cylinders with SiC-grinding paper (P320) for 30 s and with a force of 10 N at a speed of 150 rpm followed by grinding on a nylon surface with a diamante suspension (9 μm, MetaDi Supreme) and lubricant (MetaDi Fluid) for 15 min with a force of 25 N (150 rpm). Ground cylinders were polished with polishing paste (amorphous SiO_2, MasterMet 2, EcoMet 250 + AutoMet 250 from Buehler) on a microcloth surface (10 min, 25 N, 150 rpm), followed by ultrasonication in distilled water and washing with acetone. Ti foils (1 mm thickness) were polished in a similar fashion.

Before dip-coating, the Si wafers and polished Ti foils/cylinders were washed with ethanol. Dip-coating was performed in a dip-coater (idLAB) under controlled atmosphere at a temperature of 25 °C and a relative humidity of 40%. After dip-coating the samples were dried for 4 h at 80 °C in a preheated tube furnace under air. The dried samples were then calcined in the same tube furnace under air flow heating at 1.0 K/min to 475 °C, holding this temperature for 20 min, and then cooling naturally to room temperature.

Physico-chemical Material Characterization. The surface morphology of the mesoporous mixed oxide films was analyzed by scanning electron microscope (JEOL 7401F) at an acceleration voltage of 10 kV and at a working distance of 4 mm. To determine the pore diameter and derive FFT plots from the SEM images, the software Image J Version 1.39u (http://rsbweb.nih.gov/ij) was employed. Elemental composition of freshly coated titanium cylinders was measured by EDX (Bruker Quantax 400) attached to the SEM at an accelerating voltage of 5 kV. Transmission electron micrographs (TEM) were recorded on a FEI Tecnai G^2 20 S-TWIN instrument operated at 200 kV on film samples scraped off from the Ti substrates.

2-D SAXS patterns were measured in transmission mode on oxide films coated onto thin titanium foils (11.4 μm) at beam incident angle of β = 90° and β = 7° with respect to the film surface. The SAXS patterns were recorded at the HASYLAB B1 Beamline at DESY Hamburg at a sample detector distance of 3589 mm and calibrated radiation energy of 16 keV using a 2D PILATUS 1 M detector. The SAXS data were processed employing the computer program FIT2D. Coated Ti foils and cylinders were analyzed by XRD on a Bruker D8 Advance instrument (Cu Kα radiation). The average crystallite size was calculated applying the Scherrer equation.

Krypton adsorption isotherms for the porous oxide coatings were measured at 77 K with a Quantachrome Autosorb-1-C. Prior to adsorption, the samples were degassed in vacuum at 80 °C for 2 h. Specific surface areas were calculated from the Brunauer–Emmett–Teller (BET) method. To facilitate a direct comparison, the derived absolute surface area was then related to the geometrical area (planar dimensions) of the coated substrate. To determine the mass of catalytic coatings, the oxide films were dissolved in a mixture of H_2SO_4 (2 mL, 95 wt %), $NaClO_4$ (30 mg), and HCl (6 mL, 37%) at 180 °C and 18 bar in a microwave (200 W) for 30 min. The metal concentration of the clear solution was then measured by ICP-

dx.doi.org/10.1021/cs4000238 | ACS Catal. 2013, 3, 1324–1333

OES (Varian 715-ES) and used to calculate the total amount of catalyst.

Electrochemical ClER Performance. Electrochemical performance in chlorine evolution was measured on coated Ti cylinders mounted in a rotating-disc electrode (RDE) setup. Experiments were conducted in a self-made single-compartment cell on a rotating-disk electrode from PINE Instruments at a rotation speed of 3500 rpm, at a temperature of 40 °C and under nitrogen flow (150 mL/min). A 4 M sodium chloride solution with a pH of 3 served as electrolyte. A Luggin capillary was used to minimize errors due to solution resistance in the electrolyte. Platinum gauze served as counter electrode; a reversible hydrogen electrode from Gaskatel was used as reference electrode. The electric potential was controlled with a commercial dual-channel potentiostat (Gamry Reference 3000). The voltammetric curves were recorded at potentials between 1.2 and 2 V vs RHE and with a scan rate of 5 mV/s. Tests were conducted in the regime of bubble formation. (Formation of chorine bubbles was, for example, visible for a templated 15 wt % Ir catalyst at current densities above 30 mA/cm^2 when the working disk was not rotated.)

RESULTS AND DISCUSSION

Film Morphology. By employing Pluronic F127 as pore template, mesoporous oxide coatings with compositions Ru/TiO_2, Ir/TiO_2 and Ru/Ir/TiO_2 were synthesized. For comparison coatings of identical composition were synthesized also without the mesopore template. Figure 1 presents SEM images and corresponding EDX line-scan data for templated oxide films containing (A) 15 wt % Ru, (B) 15 wt % Ir, and (C) 7.5 wt % Ru along with 7.5 wt % Ir in TiO_2. A film of composition 15 wt % Ir/TiO_2 and synthesized without the mesopore template is presented in Figure 1 D for comparison. For each film top-view SEM images are shown at magnifications of 100,000× (row 1) and 1000× (row 2). The EDX data (row 3) correspond to the SEM images in row 2 and indicate the atom ratio between noble metal and oxygen along the indicated scan line.

The SEM images of all templated films show a distinct morphology (Figure 1 A1/B1/C1). The film surfaces are completely penetrated by locally ordered mesopores. The mesopores possess a diameter of about 8−10 nm. The thickness of the mesopore walls amounts to about 3−5 nm. Moreover, FFT-transformations of the SEM images (insets in Figure 1 A1/B1/C1) feature homogeneous rings, which confirm that the templated mesopores are locally ordered. The positions of the rings correspond to a periodic distance of about 13 nm. Both the pore size as well as the observed pore structure correspond well with systems reported in literature for TiO_2 films that were templated with the same structure-directing agent F127 and calcined at 475 °C.[29,34] In contrast to the templated oxide films, the characteristic mesopore structure is not visible in the Ir-containing titania film synthesized without the mesopore template (Figure 1 D1). Hence, employing the amphiphilic block-copolymer F127 in the synthesis of Ir- and Ru-containing titania films results in a film morphology that is typical of micelle-templated metal oxide coatings. However, a direct comparison between SEM images of the different templated films (Figure 1 A1/B1/C1) reveals that with increasing content of ruthenium (B1 → C1 → A1) the pore systems shows a slightly more sintered appearance. The synthesized films are macroscopically homogeneous in morphology and compositions. SEM images recorded at a magnification of 1000× on the different templated films evidence a smooth film surface (Figure 1 A2/B2/C2). The films are devoid of macroscopic cracks. Moreover, the corresponding EDX spectra recorded as line scans over a length of 120 μm in the imaged areas (Figure 1 A3/B3/C3) show in all three cases a constant metal content along the scan line. Also the film synthesized without the mesopore template shows a similar Ir distribution in the EDX line scan (Figure 1 D3). Hence phase separation between the added noble metal and the TiO_2 matrix can be ruled out within the lateral resolution limits of SEM-EDX, i.e., on a scale of about 0.5 μm. The template-based synthesis of titania films containing up to 15 wt % Ru, Ir, or Ru and Ir therefore produces macroscopically crack-free films with templated porosity and with a homogeneous distribution of the added noble metal inside the mesoporous TiO_2 matrix.

Pore Structure. The ordering of templated mesopores in the volume of the templated films was studied by SAXS on films containing 15 wt % of either Ru (A), Ir (B), or Ru + Ir (C). All films were analyzed after thermal treatments at 300 (no. 1, no. 2) and 475 °C (no. 3, no. 4), respectively. Figure 2 presents the corresponding 2D-SAXS patterns recorded at beam incident angles perpendicular (β = 90°, no. 1, no. 3) and at β = 7° (no. 2, no. 4) relative to the substrates surface.

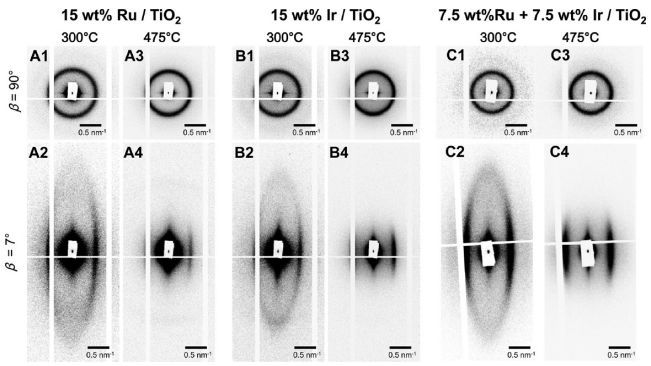

Figure 2. 2D SAXS analysis of mesoporous titania films templated with F127 containing (A) 15 wt % Ru, (B) 15 wt % Ir, and (C) 7.5 wt % Ru + 7.5 wt % Ir. Films were analyzed after thermal treatment at either 300 °C (no. 1, no. 2) or 475 °C (no. 3, no. 4). All images recorded in transmission mode with a beam incident angle of β = 90° (no. 1, no. 3) and β = 7° (no. 2, no. 4) with respect to the film surface. All films were dip-coated at 60 mm/min onto titanium foil.

The SAXS image recorded at β = 90° for the 15 wt % Ru/TiO_2 calcined at 300 °C (Figure 2 A1) clearly shows an isotropic diffraction ring which indicates ordering of the templated mesopores perpendicular to the substrate surface. The ring position corresponds to a *d*-spacing of 13 nm. In contrast, SAXS data recorded at β = 7° form an elliptical pattern with *d*-spacings corresponding to 13 nm (in-plane) and 5 nm (off-plane) (Figure 2 A2). Both observed SAXS patterns are consistent with EISA-derived distorted cubic mesopore structures. The observed anisotropic deformation of the pore lattice can be attributed to shrinkage of the oxide film perpendicular to the substrate due to volume losses that are induced by sample drying and calcination. Calcination at a higher temperature of 475 °C results in slightly different diffraction patterns. SAXS recorded at β = 90° still shows an isotropic ring (Figure 2 A3) and a similar *d*-spacing of about 14 nm. However, the elliptical diffraction ring observable at β = 7°

dx.doi.org/10.1021/cs4000238 | ACS Catal. 2013, 3, 1324−1333

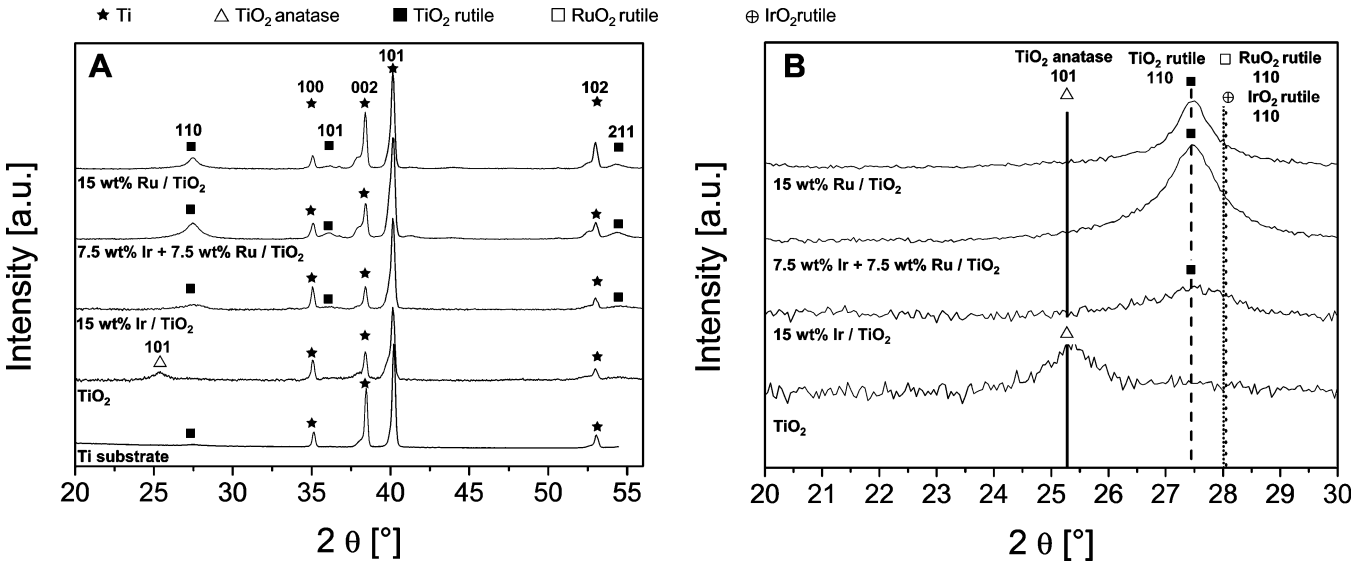

Figure 3. XRD analysis of F127-templated TiO_2 films containing 15 wt % Ir, 7.5 wt % Ir + 7.5 wt % Ru, and 15 wt % Ru. The uncoated (but calcined) substrate and a F127-templated pure TiO_2 film are shown for comparison. Symbols and lines indicate reference reflection positions reported in the literature: TiO_2 (■, rutile, PDF-No. 00-021-1276), TiO_2 (△, anatase, PDF-No. 00-021-1272), Ti (★, PDF-No. 00-044-1294), RuO_2 (□, PDF-No. 00-040-1290), and IrO_2 (⊕, PDF-No. 00-015-0870). All films were dip-coated onto titanium substrates and calcined at 475 °C.

is not fully closed anymore (Figure 2 A4), indicating the beginning degradation of the pore system.

A corresponding behavior as observed here for 15 wt % Ru/TiO_2 has been reported before by Grosso et al. for pure titania.[35] They synthesized TiO_2 in a similar procedure based also on $TiCl_4$ and the same template F127, but without the addition of ruthenium acetate, and studied the mechanistic aspects of film deposition and calcination in detail. They observed similar ring (β = 90°) and ellipsoidal patterns (β = 4°) for films dip-coated at a relative humidity of 20%.[35] The SAXS pattern observed by Grosso et al. for titania was attributed to the presence of a body-centered cubic mesopore system oriented with the (110) direction normal to the substrate surface. Observing diffraction rings instead of individual reflection spots can be explained by slight distortion of the pore order typical for dip-coating at the low humidity as well as by the size of the ordered mesopore domains being smaller than the area analyzed by the incoming X-ray beam.

Moreover, Grosso et al. reported that at calcination temperatures of about 500 °C the cubic mesopore structure of titania transforms into an ordered mesopore arrangement with grid-like structure.[35] This transition into a grid-like structure led to a significant decrease in intensity of the off-plane reflection. A similar effect is seen in the present study for 15 wt % Ru/TiO_2 calcined at 475 °C as indicated by disappearance of the off-plane contribution from SAXS patterns recorded at (β = 7°) (Figure 2 A4). Thus, the synthesis of micelle-templated Ru/TiO_2 films with cubic as well as grid-like mesopore structure from solutions containing $TiCl_4$ and F127 succeeds despite the presence of ruthenium acetate in the coating solution.

A similar pore ordering and calcination behavior of the templated pore system as observed for Ru/TiO_2 can be seen also for titania films containing either 15 wt % Ir (Figure 2 B1−4) or a combination of 7.5 wt % Ir and 7.5 wt % Ru (Figure 2 C1−4). The films of nominal composition 15 wt % Ir/TiO_2 feature after calcination at 300 °C (Figure 2 B1) as well as 475 °C (Figure 2 B3) isotropic diffraction rings corresponding to a d-spacing of 14 nm (β = 90°). When analyzed at β = 7° the film calcined at 300 °C produces an ellipsoidal diffraction pattern ($d_{\text{in-plane}}$ = 14 nm, $d_{\text{off-plane}}$ = 4 nm), whereas the film calcined at 475 °C shows an incomplete ellipse ($d_{\text{in-plane}}$ = 14 nm). Similar patterns are observed also for the Ru+Ir/TiO_2 film analyzed at β = 90° (d = 13 nn) and at β = 7° ($d_{\text{in-plane}}$ = 13 nm, $d_{\text{off-plane}}$ = 5 nm). Hence, all studied films that contain 15 wt % of either Ru, Ir, or Ru+Ir feature the same pore structure and lattice parameters that differ only within the experimental accuracy. The proposed synthesis based on $TiCl_4$ and F127 therefore facilitates the addition of ruthenium acetate or iridium acetate up to a metal loading of at least 15 wt % without significant modification or degradation of the templated mesopore system.

Composition of the Mesopore Walls. The phase composition of the mesopore walls was investigated by X-ray diffraction (XRD), transmission electron microscopy (TEM), and selected area electron diffraction (SAED). Diffractograms recorded on Ti substrates coated with micelle-templated titania films containing 15 wt % of either Ru, Ir, or Ru + Ir are shown in Figure 3 A. For comparison diffractograms are provided also for micelle-templated pure titania films as well as uncoated Ti substrates (Figure 3 A). Figure 3 B presents in addition the 2Θ range between 20° and 30° at higher resolution for all titania-based films. Symbols indicate the major reflections assigned to the different possible crystal phases reported in literature.

The uncoated titanium substrates show after calcination at 475 °C strong reflections at positions of 35.07°, 38.41°, 40.17° and 53.00° (Figure 3 A ″Ti substrate″). The reflections can be unambiguously assigned to the crystal planes in (100), (002), (101), and (102) orientation reported for titanium (PDF-No. 00-044-1294). In addition also a small peak at 27.45° can be observed. This peak position agrees well with the (101) reflection reported for the rutile phase of TiO_2 and probably forms as an overlayer during calcination of the cleaned titanium substrate at 475 °C. However, the contribution of TiO_2 rutile is rather small compared to the signals resulting from the metallic Ti substrate.

dx.doi.org/10.1021/cs4000238 | ACS Catal. 2013, 3, 1324−1333

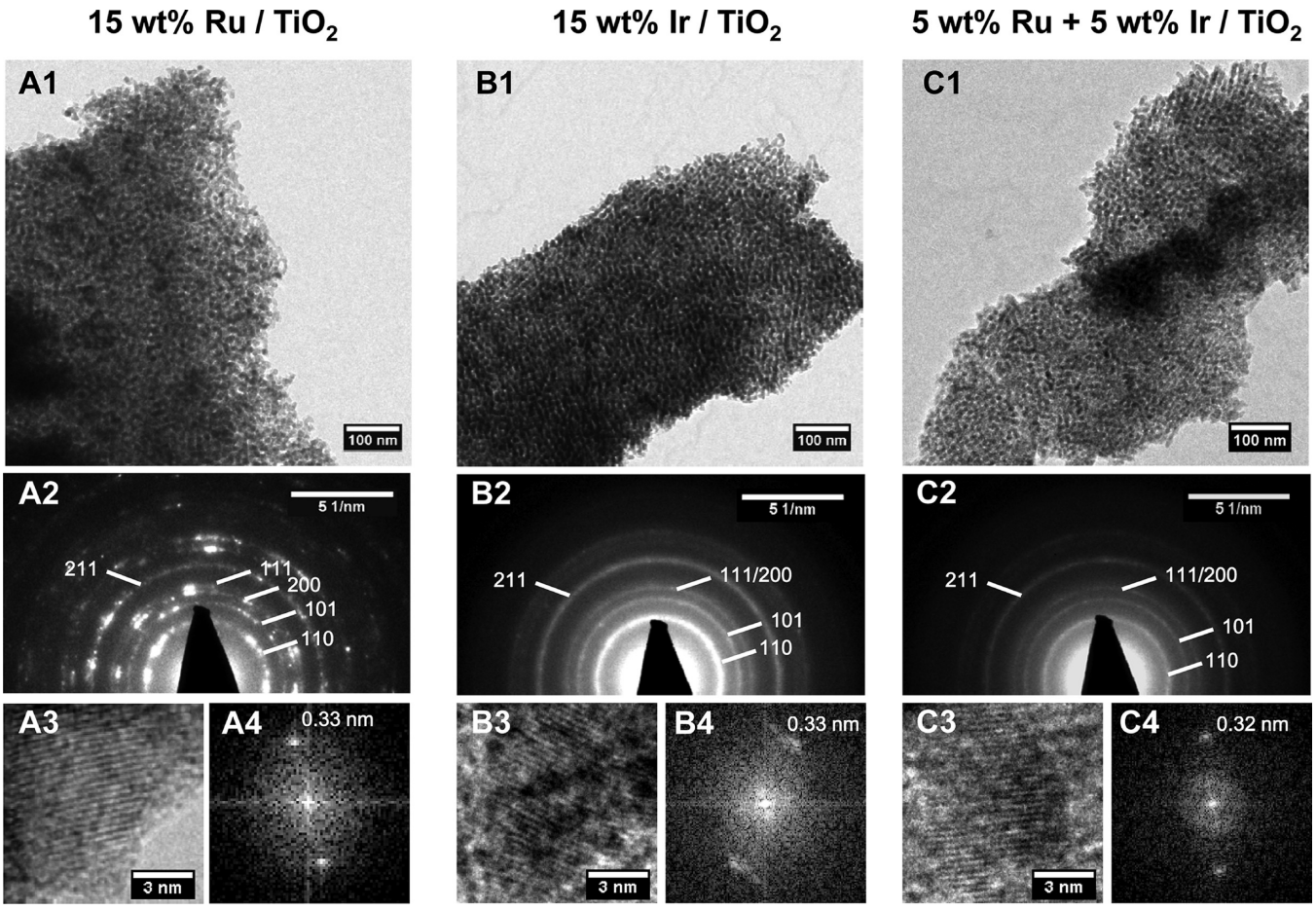

Figure 4. TEM and SAED analysis of F127 templated TiO_2 films containing different amounts of Ru and Ir: (A) 15 wt % Ru, (B) 15 wt % Ir, and (C) 5 wt % Ru + 5 wt % Ir). TEM images (A1−C1) are shown along with the corresponding SAED data (A2−C2), HR-TEM image (A3−C3), and the respective FFT plots (A4−C4). All films were dip-coated onto titanium substrates at 60 mm/min and calcined at 475 °C. (Indexing refers to TiO_2 rutile.).

A micelle-templated pure TiO_2 film coated onto a cleaned Ti substrate (Figure 3 A ″TiO_2″) shows after calcination at 475 °C the same contributions that can be assigned to titanium. In addition a broad reflection at 25.36° becomes evident (positions obtained from peak fitting). This reflection can be assigned to the anatase phase of TiO_2 (PDF-No. 00-021-1272) with a crystallite size of about 9.0 nm (from Scherrer equation applied to the (101) reflection). Both the phase assignment as well as crystallite size agrees well with observation reported in literature for micelle-templated TiO_2 films synthesized from $TiCl_4$ precursors.[30,35]

The films that contain added noble metals ruthenium or iridium show a different behavior. All reflections originating from the titanium substrate are clearly visible also in the diffractograms recorded for mesoporous 15 wt % Ir/TiO_2 film (Figure 3 A). However, the signal corresponding to TiO_2 anatase is not present. Instead broad reflections at 27.44°, 36.11°, and 54.61° are observed. A similar diffraction pattern is detected also for the coating titania containing 7.5 wt % Ru with 7.5 wt % Ir (Figure 3 A). The broad reflections are located at similar positions, i.e. 27.44°, 36.06° and 54.38°. An almost identical pattern is recorded also for the film containing 15 wt % Ru with broad reflections at 27.47°, 36.11° and 54.35. All three signals correspond well with the reflections (110), (101), and (211) of TiO_2 in rutile structure (PDF-No. 00-021-1276).

The phase assignment for the crystalline phases becomes clearer from Figure 3 B, which displays the sections of the diffractograms between 20° and 30°. Vertical lines in Figure 3 B indicate the reflection positions for all phases that can be potentially formed by the employed film composition. The potentially formed crystalline phases are TiO_2 anatase (25.28°, PDF-No. 00-021-1272), TiO_2 rutile (27.45, PDF-No. 00-021-1276), RuO_2 rutile (28.01°, PDF-No. 00-040-1290), and IrO_2 rutile (28.06°, PDF-No. 00-015-0870). A comparison of these literature values with the experimentally observed reflection positions shows that for all three cases where either Ir or Ru or both were added to the film synthesis TiO_2 rutile is the formed crystalline phase, not TiO_2 anatase nor IrO_2 or RuO_2 (Figure 3 B). Hence, addition of small amounts of Ir or Ru induces a change in the oxides phase composition from anatase (pure TiO_2) into rutile, indicating the formation of mixed oxide crystals in rutile structure that constitute the walls of the templated mesopores.

To prove the formation of mixed oxide crystals, we compared the experimental (110) lattice parameters with the theoretical values calculated by Vegards rule. The experimental (110) lattice constants are 3.248 ± 0.006 Å (15 wt % Ir), 3.248 ± 0.001 Å (7.5 wt % Ru + 7.5 wt % Ir), and 3.245 ± 0.001 Å (15 wt % Ru). Respectively, the theoretical calculated values are 3.242, 3.241, and 3.239 Å. Hence, the behavior of the studied mixed metal oxides is consistent with Vegards rule within the

dx.doi.org/10.1021/cs4000238 | ACS Catal. 2013, 3, 1324−1333

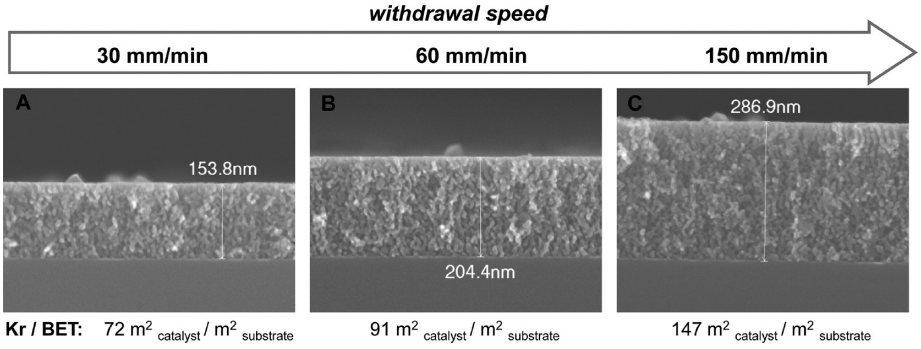

Figure 5. Analysis of film thickness (SEM) and surface area (Kr physisorption) of F127 templated 15 wt % Ir/TiO_2 films as a function of withdrawal speed applied in film deposition via dip-coating. Film thickness was measured from cross section SEM images recorded at a magnification of 100,000×. Surface area was obtained from Kr physisorption analysis. Layer thickness increases as expected with increasing withdrawal rate up. The surface area of the catalytic coatings increases accordingly. All films were calcined at 475 °C.

limits of experimental accuracy. Formation of $Ir-Ru-TiO_x$ mixed oxides in rutile structure is also the expected phase behavior according to literature reports of Gugliemi et al.[36] and Takasu et al.[8] and relates to the fact that the rutile phases of TiO_2, IrO_2, and RuO_2 are very similar in crystal structure as well as elementary cell dimensions.

However, the formed rutile phases of the different studied oxides differ in the obtained average crystallite size. Crystallite sizes estimated by Scherrer equation from the (110) rutile reflections amount to 4.6 nm (15 wt % Ir/TiO_2), 7.9 nm (7.5 wt % Ru + 7.5 wt % Ir/TiO_2), and 11.4 nm (15 wt % Ru/TiO_2), respectively. Hence, addition of Ru promotes the formation of slightly larger crystallites and therefore facilitates sintering of the pore walls. This tendency toward promoted crystallite growth can be seen also in the SEM images presented in Figure 1 for the templated films loaded with the different metals. The SEM images clearly indicate that with increasing content of ruthenium (B1 → C1 → A1) the appearance of the pore system of films calcined at 475 °C becomes more sintered and the circular pore shapes are less pronounced. However, the wall forming crystallites remained in all three cases small enough to be able to form a mixed oxide phase with template-controlled mesoporosity.

The phase composition of the formed mesopore walls was further analyzed by TEM and SAED. Figure 4 shows for mesoporous titania-based coatings containing (A) Ru, (B) Ir, and (C) Ru + Ir the obtained TEM images (no. 1), SAED diffraction pattern (no. 2), HR-TEM images (no. 3) along with the corresponding FFT image (no. 4).

The TEM images confirm for all three samples that also the complete volume of the oxide films exhibit the templated mesoporosity (Figure 4 A1, B1, C1). Moreover, SAED demonstrates for all samples very similar diffraction patterns, which can be indexed according to a TiO_2 rutile phase (Figure 4 A2, B2, C2). Hence, electron diffraction confirms the XRD-based assignment of a crystalline rutile phase. However, with increasing content of ruthenium the diffraction pattern transform from homogeneous rings (Figure 4 C2) into rings with additional individual reflection spots (Figure 4 A2). This observation is in agreement with the XRD analysis (Figure 3) and can be rationalized by an increase in crystallite size with increasing ruthenium content, where larger crystals show stronger diffraction signals. Moreover, HR-TEM demonstrates that the pore walls are composed of individual oxide crystals for all three oxides. In all three cases lattice planes can be identified (Figure 4 A3, B3, C3) and a lattice constant of about 0.32 to 0.33 nm is obtained (Figure 4 A4, B4, C4). The obtained lattice constants correspond well to (110) rutile, which further supports the phase assignment to a rutile phase. Hence, mesoporous titania films containing either ruthenium, iridium, or both are completely mesoporous after calcination at 475 °C and composed of nanocrystals with rutile structure.

Control over Film Thickness and Surface Area. To illustrate facile control over thickness and total surface area of the catalytic layers, films containing 15 wt % Ir were synthesized via dip-coating at different withdrawal speeds, calcined at 475 °C, and analyzed with Kr physisorption. Figure 5 shows cross-section SEM images of the obtained films along with the resulting values of surface area normalized to the same planar area of the substrate.

When the withdrawal speed was increased from 30 to 60 and 150 mm/min the thickness of the calcined films increases from 154 to 204 and 287 nm, respectively. This increase is in agreement with literature reports[37] and explained by a larger amount of synthesis solution trapped on the substrate during faster film deposition. With increasing film thickness the specific Kr-BET surface area related to the volume of the coatings ($m^2_{catalyst}$ per $cm^3_{coating}$) remained almost constant between 468, 446, and 512 m^2/cm^3, respectively, whereas the measured total surface area of the oxide coating increases with film thickness. Dip-coating at 30 mm/min results in 72 $m^2_{catalyst}$ per $m^2_{substrate}$, and the film dipped at 150 mm/min possesses a surface area twice as high (147 $m^2_{catalyst}$ per $m^2_{substrate}$). Hence, a doubling in film thickness also doubles the provided surface area as expected for the synthesis of oxide films with homogeneous templated porosity.

On the basis of the presented analysis by SEM, TEM, SAXS, XRD, SAED, and Kr physisorption, the successful synthesis of templated mesoporous titania coatings containing up to 15 wt % of iridium, ruthenium, and combinations of both metals can be concluded. The templated pores are open and locally ordered and transform from cubic (T_{calc} = 300 °C) to a grid-like structure at increased calcination temperatures (T_{calc} = 475 °C). The pore walls consist of nanocrystalline rutile phases of mixed oxides $Ir-Ti-O_x$, $Ru-Ti-O_x$, or $Ru-Ir-Ti-O_x$, respectively. The obtained crystallite size depends on the amount of added noble metal and increases with increasing ruthenium content. The films are homogeneous and macroscopically crack-free. The films' total surface area scales with film thickness and can be easily adjusted by changing the withdrawal speed employed for dip-coating. The catalytic coatings represent therefore model systems with easily tunable parameters and can be used

dx.doi.org/10.1021/cs4000238 | ACS Catal. 2013, 3, 1324−1333

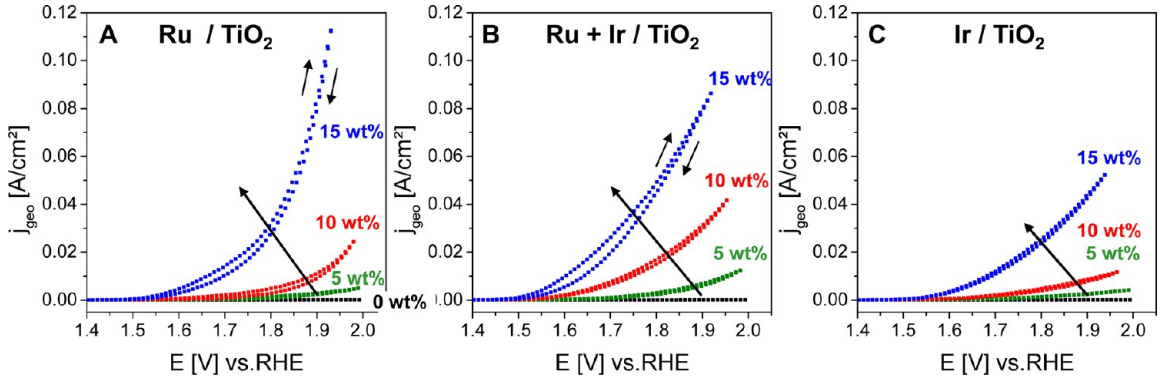

Figure 6. Cyclovoltammograms for chlorine evolution over mesoporous templated TiO_2-based catalysts containing different amounts of (A) Ru, (B) Ru + Ir, and (C) Ir. All films were templated with F127, dip-coated at identical conditions and calcined at 475 °C. Added noble metal content amounts to 0 wt % (black), 5 wt % (green), 10 wt % (red), and 15 wt % (blue), respectively. Experimental conditions: 4 M NaCl solution, pH = 3, T = 40 °C, scans from 1.2 to 2 V at the same forward and reverse scan rate of 5 mV/s, 3500 rpm, reversible hydrogen reference electrode, Pt wire counter electrode.

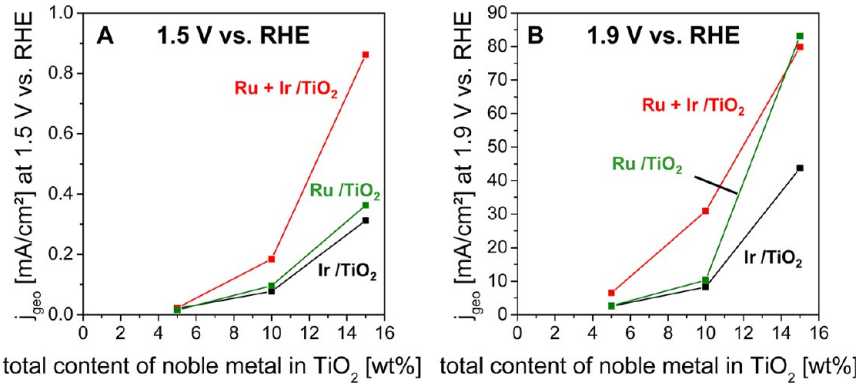

Figure 7. Current density at potentials of (A) 1.5 V and (B) 1.9 V vs RHE measured for chlorine evolution over mesoporous TiO_2-based catalysts as a function of the nominal content of noble metal Ir (black), Ru (green), or Ir + Ru (1:1, red). All samples templated with F127 and calcined at 475 °C. Experimental conditions: 4 M NaCl solution, pH = 3, T = 40 °C, scan rate = 5 mV/s, 3500 rpm, reversible hydrogen reference electrode, Pt wire counter electrode.

to elucidate structure–activity relationships in electrocatalytic reactions.

Influence of Catalyst Composition and Templated Porosity on the Catalytic ClER Performance. ClER performance of the developed electrode coatings was studied by cyclovoltammetry. Compositions, film thickness, and templated porosity of the catalytic electrode coatings were systematically varied in order to identify relevant influence parameters and to optimize the catalytic performance. Figure 6 depicts cyclovoltammetry curves recorded in ClER on mesoporous templated catalysts containing a total content of 5, 10, and 15 wt % of either Ru (Figure 6 A), equal concentration of Ru and Ir (Figure 6 B), or Ir (Figure 6 C). All current densities were normalized to the surface area of the substrate, i.e. the geometrical surface area of the uncoated tianium cylinder.

All CV curves recorded on the different Ir- and Ru-containing mesoporous TiO_2 catalysts show the same general behavior. At potentials below ca. 1.5 V no reaction takes place (Figure 6 A–C). This behavior is expected, since 1.44 V vs RHE represents the thermodynamic minimum potential for ClER evolution under the studied conditions (Nernst equation, 40 °C, 10^{-2} bar, pH = 3). However, potentials exceeding 1.5 V vs RHE cause a steady increase in measured current density, which indicates chlorine formation. Hence, all synthesized Ru- and Ir-containing catalysts are active in ClER. In contrast, reference experiments on mesoporous TiO_2 containing neither Ru nor Ir did not show a measurable current density in the whole studied potential range (Figure 6 A, ″0 wt %″). The presence of Ir and Ru is therefore responsible for the observed catalytic ClER activity. Moreover, the reaction is not transport limited in the studied potential range as indicated by the absence of the current decreases at high potentials.

The recorded CV backward and forward scans provide identical current densities for catalysts containing up to 5 wt % Ru (Figure 6 A), 10 wt % combined Ir and Ru (Figure 6 B), or up to 15 wt % Ir (Figure 6 C). However, a slight hysteresis can be seen for catalysts that contain higher ruthenium loadings. One possible explanation for the observed hysteresis could be capacitive effects at the electrode–solution interface: a higher capacitance of Ru-containing electrodes compared to Ir-containing electrodes can result in a more pronounced hysteresis in the CV of Ru containing samples. The studied catalysts differ systematically in their overall activity. In all cases a significant increase in current density can be seen with increasing content of either Ru (Figure 6 A), Ir (Figure 6 C), or a combination of both metals (Figure 6 B). Hence, adding higher amounts of the respective acetate precursor of ClER-active metals to the $TiCl_4$-based synthesis solutions results in catalysts with increasingly higher activity, even at active metal

dx.doi.org/10.1021/cs4000238 | ACS Catal. 2013, 3, 1324–1333

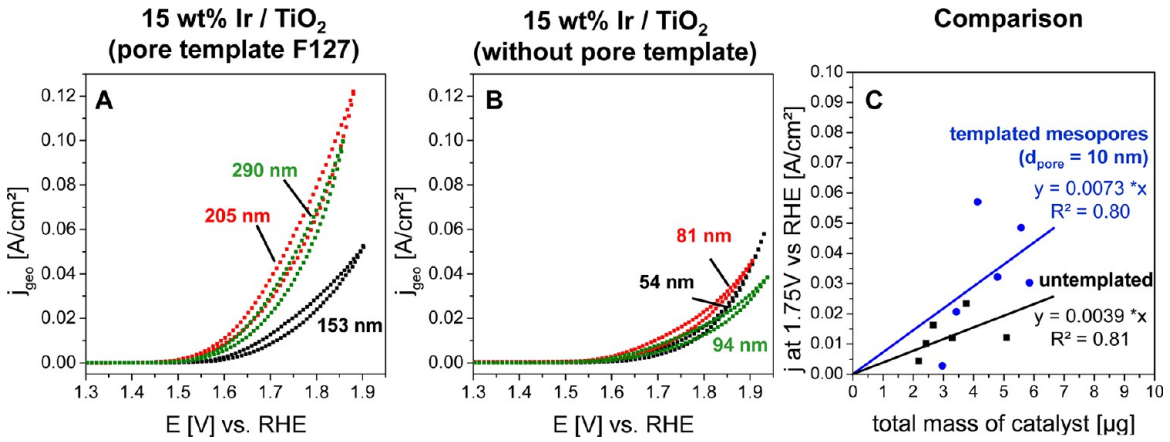

Figure 8. Comparison of performance in chlorine evolution for 15 wt % Ir/TiO_2 catalysts with and without templated mesopores and with controlled variation of the thickness of the catalyst films. (A) CVs measured for 10 nm pores templated with F127. (B) CVs measured for untemplated catalysts. (C) Geometric current density compared at a potential of 1.75 V vs RHE plotted as a function of the mass of the respective catalytic coating determined from ICP. All templated samples synthesized with F127. All films calcined at 475 °C. Experimental conditions: 4 M NaCl solution, pH = 3, T = 40 °C, scan rate = 5 mV/s, 3500 rpm, reversible hydrogen reference electrode, Pt wire counter electrode.

loadings as high as 15 wt %. The added noble metal can therefore be fully utilized to increase catalyst performance.

The trends in catalytic activity become more evident when comparing all catalyst at the same applied potential. Figure 7 plots current densities (normalized to the substrates geometric surface area) for all studied catalysts as a function of their content of active metal. Catalysts are compared at two different potentials, i.e., near the ClER onset potential (1.5 V vs RHE, Figure 7A) and at higher current densities that reflect better the conditions of practical ClER applications (1.9 V vs RHE, Figure 7 B).

In all studied cases the observed activity increases with the amount of active metal. A comparison of current densities obtained for the different metals at low potentials (Figure 7 A) shows that activity increases in the order of Ir, Ru, and the combination Ru+Ir. This general trend is confirmed also at higher potentials (Figure 7 B). However, at high loadings and high potentials the Ru-based catalyst becomes more active than both Ir and the bimetallic combination.

The observed influences of catalyst composition compare well with literature reports on catalysts without templated mesopore structure. Kuhn et al. investigated the ClER performance of different RuO_2–TiO_2 catalysts synthesized by brushing multiple layers of solutions containing ruthenium chloride and $TiCl_4$ or $Ti(OEt_4)$ onto titanium plates and calcination in air at 400 °C for 6 h.[11] Galvanostatic measurements (20 °C, 5 M NaCl) revealed that increasing Ru content increased the recorded current density. Moreover, they compared the activity of TiO_2 catalysts containing either 10 mol % Ir or Ru. Both catalysts performed similar at low current densities (j < 5 mA/cm^2), whereas current densities of ~50 mA/cm^2 indicated lower overpotentials for the $Ru_{0.1}Ti_{0.9}O_2$ catalysts. Consonni et al. compared the ClER activity of RuO_2 and IrO_2 catalysts prepared without titania by thermal decomposition of either $IrCl_3$ or $RuCl_3$ dissolved in isopropanol.[38] Galvanostatic measurements conducted in 5 M NaCl solution with 0.01 M HCl (pH = 2) at 25 °C indicate for the whole studied potential range (1.24–1.34 V vs NHE) RuO_2 to be slightly more active than IrO_2.

In order to study also the effect of the templated pore system on ClER performance, catalysts with the same composition but with different content of templated mesopores and with different film thickness were synthesized. Due to its high activity and stable performance 15 wt % Ir/TiO_2 was selected as catalyst composition. Figure 8 A presents cylcovoltammetry data recorded in ClER on mesoporous templated 15 wt % Ir/TiO_2 films with film thickness systematically varied between 153 and 290 nm by dip-coating at different withdrawal speeds of 30, 60, and 150 mm/min. Figure 8 B provides for comparison CV data obtained on films that were synthesized without templates, i.e., films that did not contain micelle-templated mesopores. Figure 8 C directly compares the performance of catalysts with and without templated mesopores by plotting the recorded current density at a potential of 1.75 V vs RHE as a function of catalyst mass.

The CV data indicate for all catalysts a similar activity behavior, i.e., progressively increasing current densities at potentials exceeding 1.5 V vs RHE. Moreover, both types of catalysts show a clear tendency toward higher current densities when film thickness is increased (Figure 8 A,B). This effect can be rationalized by the fact that the total amount of available catalyst increases with film thickness, whereas the surface area used for normalization, i.e., the geometric planar surface area of the electrode substrate, remains constant. Thicker films correspond to a higher surface area (see Figure 5), and hence more active sites can be utilized in thicker films and current densities increase.

However, catalysts with templated and untemplated pore systems differ significantly in mass-related activity. Figure 8 C plots the current density measured at 1.75 V/RHE vs the total mass of catalyst for both types of materials. Despite the scatter in experimental CV data an increase in current densities with increasing catalyst mass is clearly evident. Moreover, for the same mass of catalyst the coatings containing templated mesopores provide twice as high current densities as coatings without templated mesopores. Thus, the additional meso-porosity introduced by pore templating enables a significantly better utilization of the available catalyst material.

CONCLUSIONS

We developed a method for the synthesis of chlorine evolution catalysts with improved performance. The performance increase results from the introduction of controlled meso-porosity into the pore system of Ru- and Ir-containing TiO_2

dx.doi.org/10.1021/cs4000238 | ACS Catal. 2013, 3, 1324–1333

catalysts by pore templating with micelles of amphiphilic block-copolymers. The synthesis succeeds by employing ruthenium acetate or iridium acetate in combination with $TiCl_4$ in a joined precursor solution.

Mesoporous TiO_2-based catalysts could be synthesized with up to 15 wt % of either Ru, Ir, or a combination of both active metals. The catalysts form a nanocrystalline mixed oxide with rutile structure. The addition of ruthenium promotes the formation of slightly larger crystallites. The templated mesopores of about 10 nm in diameter show local ordering in a cubic pore system and therefore good pore connectivity.

The templated mesoporosity can be exploited to increase the performance of the catalysts in electrochemical chlorine evolution. A systematic catalyst optimization reveals that titania-based catalyst films containing iridium show a more stable performance than ruthenium-containing coatings. Moreover, the coatings performance benefits also from a high loading of an active component, a high coating thickness that increases the catalyst mass and from the presence of additional mesopores that enhance the accessible active surface area.

Further investigations should address the mechanism of formation of the crystalline mixed oxides. Moreover, a systematic variation of size, spacing, and topology of templated mesopores could reveal the contribution of mass transport to the observed performance enhancement. Finally, elucidating the impact of thickness and crystallinity of the pore walls on the electric conductivity of the catalyst could pave the way for further catalyst improvement.

AUTHOR INFORMATION

Corresponding Author

*E-mail: ralph.kraehnert@tu-berlin.de.

Notes

The authors declare no competing financial interest.

ACKNOWLEDGMENTS

We thank Ulla Vainio (SAXS), Xenia Tuaev (SAXS), ZELMI at TU Berlin (TEM), Benjamin Paul (SEM), Kornelia Weh (ICP) and Tobias Reier (catalytic measurements) for valuable contributions to this study. Portions of this research were carried out beamline B1 at the light source DORIS III at DESY, a member of the Helmholtz Association (HGF). The financial support of BMBF (FKZ 03X5517A, FKZ 03EK3009) is gratefully acknowledged. Ralph Kraehnert and Peter Strasser acknowledge also financial support by the German Cluster of Excellence in Catalysis (EXC 314, UNICAT) funded by the German National Science Foundation (DFG) and managed by the Technical University Berlin.

REFERENCES

(1) EuroChlor; *Chlorine Industry Review*, 2011−2012.
(2) Huskinson, B.; Rugolo, J.; Mondal, S. K.; Aziz, M. J. *Energy Environ. Sci.* **2012**, *5*, 8690−8698.
(3) Thomassen, M.; Borresen, B.; Hagen, G.; Tunold, R. *Electrochim. Acta* **2005**, *50*, 1157−1167.
(4) Beer, H. B. *J. Electrochem. Soc.* **1980**, *127*, C303−C307.
(5) Duby, P. *JOM* **1993**, *45*, 41−43.
(6) Trasatti, S. *Electrochim. Acta* **1991**, *36*, 225−241.
(7) Trasatti, S. *Electrochim. Acta* **1987**, *32*, 369−382.
(8) Takasu, Y.; Sugimoto, W.; Nishiki, Y.; Nakamatsu, S. *J. Appl. Electrochem.* **2010**, *40*, 1789−1795.
(9) Gorodetskii, V.; Neburchilov, V. *Russ. J. Electrochem.* **2005**, *41*, 971−978.
(10) Janssen, L. J. J.; Starmans, L. M. C.; Visser, J. G.; Barendrecht, E. *Electrochim. Acta* **1977**, *22*, 1093−1100.
(11) Kuhn, A. T.; Mortimer, C. J. *J. Electrochem. Soc.* **1973**, *120*, 231−234.
(12) Hoseinieh, S. M.; Ashrafizadeh, F.; Maddahi, M. H. *J. Electrochem. Soc.* **2010**, *157*, E50−E56.
(13) Shrivastava, P.; Moats, M. S. *J. Appl. Electrochem.* **2009**, *39*, 107−116.
(14) Evdokimov, S. V. *Russ. J. Electrochem.* **2000**, *36*, 489−494.
(15) Evdokimov, S. V. *Russ. J. Electrochem.* **2000**, *36*, 236−239.
(16) Gorodetskii, V. V. *Russ. J. Electrochem.* **2003**, *39*, 650−659.
(17) Panic, V. V.; Dekanski, A.; Milonjic, S. K.; Miskovic-Stankovic, V. B.; Nikolic, B. Z. *Russ. J. Electrochem.* **2006**, *42*, 1055−1060.
(18) Chen, R.; Trieu, V.; Natter, H.; Stoewe, K.; Maier, W. F.; Hempelmann, R.; Bulan, A.; Kintrup, J.; Weber, R. *Chem. Mater.* **2010**, *22*, 6215−6217.
(19) Chen, R.; Trieu, V.; Zeradjanin, A. R.; Natter, H.; Teschner, D.; Kintrup, J.; Bulan, A.; Schuhmann, W.; Hempelmann, R. *Phys. Chem. Chem. Phys.* **2012**, *14*, 7392−7399.
(20) Chen, R. Y.; Trieu, V.; Natter, H.; Kintrup, J.; Bulan, A.; Hempelmann, R. *Electrochem. Commun.* **2012**, *22*, 16−20.
(21) Trieu, V.; Schley, B.; Natter, H.; Kintrup, J.; Bulan, A.; Hempelmann, R. *Electrochim. Acta* **2012**, *78*, 188−194.
(22) Menzel, N.; Ortel, E.; Kraehnert, R.; Strasser, P. *ChemPhysChem* **2012**, *13*, 1366.
(23) Ortel, E.; Reier, T.; Strasser, P.; Kraehnert, R. *Chem. Mater.* **2011**, *23*, 3201−3209.
(24) Brinker, C. J.; Lu, Y. F.; Sellinger, A.; Fan, H. Y. *Adv. Mater.* **1999**, *11*, 579−585.
(25) Smarsly, B.; Antonietti, M. *Eur. J. Inorg. Chem.* **2006**, 1111−1119.
(26) Sanchez, C.; Boissiere, C.; Grosso, D.; Laberty, C.; Nicole, L. *Chem. Mater.* **2008**, *20*, 682−737.
(27) Sassoye, C.; Laberty, C.; Le Khanh, H.; Cassaignon, S.; Boissiere, C.; Antonietti, M.; Sanchez, C. *Adv. Funct. Mater.* **2009**, *19*, 1922−1929.
(28) Brezesinski, T.; Wang, J.; Polleux, J.; Dunn, B.; Tolbert, S. H. *J. Am. Chem. Soc.* **2009**, *131*, 1802−1809.
(29) Crepaldi, E. L.; Soler-Illia, G.; Grosso, D.; Cagnol, F.; Ribot, F.; Sanchez, C. *J. Am. Chem. Soc.* **2003**, *125*, 9770−9786.
(30) Ortel, E.; Fischer, A.; Chuenchom, L.; Polte, J.; Emmerling, F.; Smarsly, B.; Kraehnert, R. *Small* **2012**, *8*, 298−309.
(31) Pan, J. H.; Zhao, X. S.; Lee, W. I. *Chem. Eng. J.* **2011**, *170*, 363−380.
(32) Sugimoto, W.; Makino, S.; Mukai, R.; Tatsumi, Y.; Fukuda, K.; Takasu, Y.; Yamauchi, Y. *J. Power Sources* **2012**, *204*, 244−248.
(33) Oh, S. H.; Nazar, L. F. *J. Mater. Chem.* **2010**, *20*, 3834−3839.
(34) Ortel, E.; Sokolov, S.; Zielke, C.; Lauermann, I.; Selve, S.; Weh, K.; Paul, B.; Polte, J.; Kraehnert, R. *Chem. Mater.* **2012**, *24*, 3828−3838.
(35) Grosso, D.; Soler-Illia, G.; Crepaldi, E. L.; Cagnol, F.; Sinturel, C.; Bourgeois, A.; Brunet-Bruneau, A.; Amenitsch, H.; Albouy, P. A.; Sanchez, C. *Chem. Mater.* **2003**, *15*, 4562−4570.
(36) Guglielmi, M.; Colombo, P.; Rigato, V.; Battaglin, G.; Boscoloboscoletto, A.; Debattisti, A. *J. Electrochem. Soc.* **1992**, *139*, 1655−1661.
(37) Grosso, D. *J. Mater. Chem.* **2011**, *21*, 17033−17038.
(38) Consonni, V.; Trasatti, S.; Pollak, F.; Ogrady, W. E. *J. Electroanal. Chem.* **1987**, *228*, 393−406.